Universal Chroma Subsampling Strategy for Compressing Mosaic Video Sequences With Arbitrary RGB Color Filter Arrays in H.264/AVC

Wei-Jen Yang, Kuo-Liang Chung, *Senior Member, IEEE,* Wei-Ning Yang, and Le-Chung Lin

***Abstract*—In this paper, we propose a universal chroma subsampling strategy for compressing mosaic video sequences with arbitrary red-green-blue (RGB) color filter arrays (CFAs), which are widely used in the single sensor imaging pipeline, in H.264/AVC. We first develop a modified universal demosaicing scheme, which specifically recovers the G component in the color difference domain, to recover the missing color components in the input mosaic image frames. Then, based on the transform between the RGB and the YUV color spaces, the proposed universal subsampling strategy automatically samples, by considering the significance of the U and V components for reconstructing R and B pixels, the proper U and V chroma components according to the corresponding mosaic structure. To the best of our knowledge, this is the first universal chroma subsampling strategy designed specifically for mosaic video sequences with arbitrary RGB-CFAs. Experimental results on mosaic video sequences with seven common types of the RGB-CFAs demonstrate that the proposed universal chroma subsampling strategy is superior to the conventional strategy of H.264/AVC. Moreover, integrating the proposed universal demosaicing scheme and the chroma subsampling strategy can deliver better video sequence quality.**

***Index Terms*—Arbitrary color filter arrays, chroma subsampling, demosaicing, H.264/AVC video coding, single sensor digital camera.**

I. Introduction

DIGITAL VIDEO cameras are becoming increasingly popular in the consumer electronics market. To bring down the cost, most video cameras often capture the color information using a single charge-coupled device/complementary metal-oxide-semiconductor sensor imaging pipeline [25] with the red-green-blue (RGB) color filter array (CFA) structure [26], [30]. Each pixel in the image frame of a video sequence with RGB-CFA structure has only one of the three primary color components; this kind of video sequence is called a mosaic video sequence. Seven common types of the RGB-CFAs are shown in Fig. 1. The arrangement of the color filters in the RGB-CFA, usually referred to as the mosaic structure and defined by the camera manufacturers, is required for the following video processing and can be found in the video header. Since the full-color video sequence is required for the human visual system, the two missing color components of each pixel in the mosaic image frames should be recovered by the demosaicing process, which has been studied extensively in [5]–[8], [16], [21], [22], [24], [26]–[29], [31], and [34].

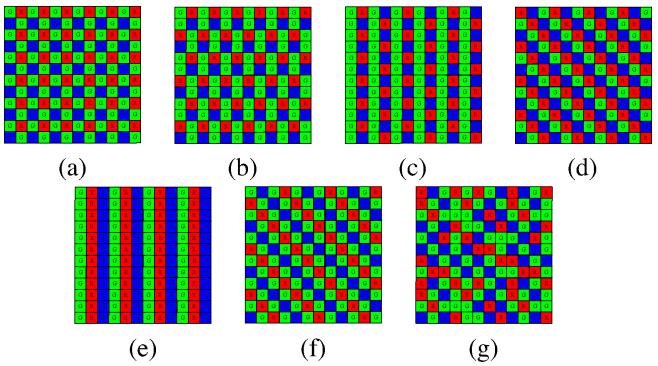

Fig. 1. RGB-CFAs. (a) Bayer CFA [1]. (b) Lukac and Plataniotis CFA [25]. (c) Yamanaka CFA [36]. (d) Diagonal stripe CFA [25]. (e) Vertical stripe CFA [25]. (f) Modified Bayer CFA [25]. (g) HVS-based CFA [32].

In addition to the demosaicing issue, the compression for mosaic video sequences has received growing attention due to the considerations of economical transmitting and storage. Some compression methods, specifically designed for mosaic video sequences with the Bayer CFA [1], [9], [38], a well-known CFA structure, have been developed [4], [11]–[13], [15]. Gastaldi *et al.* [15] proposed the first compression method for mosaic video sequences, which first partitioned a mosaic image frame into three color planes, and then applied the MPEG-2-like [19] video coder to the rearranged color planes. This method yielded limited compression performance for P-frames due to the severe aliasing of a mosaic image frame. Doutre and Nasiopoulos [11] and Doutre *et al.* [12] developed compression methods based on the H.264/AVC [14] by exploiting the motion compensation to relieve the aliasing effect, resulting in better compression performance, especially in the cases of high bitrate. Doutre and Nasiopoulos [13] presented an efficient compression method by utilizing

Manuscript received December 12, 2011; revised April 14, 2012; accepted June 19, 2012. Date of publication August 3, 2012; date of current version April 1, 2013. This work was supported by the National Science Council of Taiwan, under Contract NSC99-2221-E-011-078-MY3. This paper was recommended by Associate Editor S. Takamura.

W.-J. Yang, K.-L. Chung, and L.-C. Lin are with the Department of Computer Science and Information Engineering, National Taiwan University of Science and Technology, Taipei 10672, Taiwan (e-mail: wjyang@mail.ntust.edu.tw; klchung01@gmail.com; watery01@hotmail.com).

W.-N. Yang is with the Department of Information Management, National Taiwan University of Science and Technology, Taipei 10672, Taiwan (e-mail: yang@cs.ntust.edu.tw).

Color versions of one or more of the figures in this paper are available online at http://ieeexplore.ieee.org.

Digital Object Identifier 10.1109/TCSVT.2012.2210805

the modified H.264 intra prediction scheme for mosaic video sequences. Chen *et al.* [4] compressed the Bayer CFA video sequences by an adjusted chroma subsampling method in the H.264 video coder, which calculated the U and V chroma values for the B and R pixels in the Bayer CFA, respectively. Chen *et al.*'s method can produce significant enhancement in the quality of the reconstructed mosaic video at both the cases of high and low bitrates when compared with a conventional method in H.264/AVC, leading to a pioneer achievement in compressing Bayer CFA video sequences. Then, Chung *et al.* [10] extended the chroma subsampling method to deal with the digital time delay and integration (DTDI) CFA video sequences [3], [37], which is captured by line-scan cameras based on the Bayer CFA structure and field programmable gate arrays. Since these existing compression methods are specifically designed for mosaic sequences with the Bayer CFA-related structures, they cannot be used directly for compressing mosaic video sequences with different CFA structures due to the constraint on the mosaic structure. To alleviate the aliasing effect, non-Bayer CFAs are often used and are getting increasingly popular in digital video cameras. Thus, compressing difference types of mosaic video sequences is important and should be addressed. Existing subsampling strategies in compression methods for mosaic video sequences heavily depend on the mosaic structures, indicating that developing a universal subsampling strategy is not trivial. We propose a universal subsampling strategy that automatically samples the appropriate chroma components according to the corresponding mosaic structure recognized from the video header, instead of sampling the fixed chroma components in the conventional subsampling strategies, and hence can tackle the mosaic video sequences with arbitrary mosaic structures. Specifically, we propose a universal chroma subsampling strategy for compressing mosaic video sequences with arbitrary RGB-CFAs in H.264/AVC. In addition, the universal demosaicing scheme used in the compression method can significantly affect the quality of reconstruction video sequences. The universal demosaicing scheme proposed by Lukac and Plataniotis [26] is the most well-known scheme due to its simplicity and efficiency. Although the compression method using Lukac and Plataniotis' universal demosaicing scheme can achieve good quality of the reconstruction video sequence, the performance of the demosaicing scheme can be further enhanced by recovering the G component in the color difference domain, leading to better quality of the reconstructed video sequences. Therefore, we propose a modified universal demosaicing scheme, which specifically recovers the G component in the color difference domain, to improve the quality of the reconstructed video sequences.

Instead of using Lukac and Plataniotis' demosaicing scheme [26], the proposed method first develops a modified universal demosaicing scheme, which specifically recovers the G component in the color difference domain, to recover the two missing color components in the image frames. Then, based on the transform between the RGB and YUV color spaces, the proposed universal subsampling strategy automatically selects, by considering the significance of the U and V components for reconstructing R and B pixels, the proper pixels to sample the U and V chroma components according to the corresponding mosaic structure, leading to better quality of the reconstructed mosaic video sequences. To the best of our knowledge, this is the first universal compression method designed specifically for mosaic video sequences with arbitrary RGB-CFAs. The experimental results on the mosaic video sequences with seven common types of the RGB-CFAs demonstrate that the proposed universal chroma subsampling strategy delivers better quality of the reconstructed mosaic video sequences than the conventional strategy of H.264/AVC. Furthermore, integrating the proposed universal demosaicing scheme and chroma subsampling strategy can deliver better video sequence quality. We summarize the major contributions of our paper as follows. First, we propose a modified universal demosaicing scheme, which specifically recovers the G component in the color difference domain, to improve the quality of the reconstructed video sequences. Second, we develop the first universal chroma subsampling strategy for compressing the mosaic video sequences with arbitrary RGB-CFAs in H.264/AVC.

The remainder of this paper is organized as follows. In Section II, a modified universal demosaicing scheme is proposed. In Section III, we describe the traditional chroma subsampling strategy in H.264/AVC and point out its drawback. In Section IV, we present the proposed a universal chroma subsampling strategy for compressing mosaic video sequences with arbitrary RGB-CFAs. Section V reports the experimental results on the quality of the reconstructed mosaic video sequences with seven common types of RGB-CFAs. Section VI presents concluding remarks.

II. Modified Universal Demosaicing Scheme

Before sampling the chroma components by the proposed universal subsampling strategy, we should recover, by using universal demosaicing schemes, the two missing components in the mosaic image, as they appeared in the universal demosaicing schemes [26], [31]. Among the developed universal demosaicing schemes, Lukac and Plataniotis' universal RGB-CFA demosaicing scheme [26] is the most well-known scheme due to its simplicity and efficiency. However, Lukac and Plataniotis' scheme recovers the missing R and B components in the color difference domain but recovers the missing G component in the spatial domain. Recovering the G component in the spatial domain often causes large interpolation errors, leading to the degradation of the demosaiced video quality. To mitigate the degradation, Lukac and Plataniotis' scheme uses a color correlation-driven postprocessing step to address the limitations of the recovering step in the spatial domain. Although the postprocessing step may reduce the degradation, the recovery step has a more substantial effect with respect to the quality of the demosaiced video sequences, implying that some modification in the recovery step may lead to substantial improvement. Since the contrast in the color difference domain is much less than that in the spatial domain, recovering G component in the color difference domain can result in smaller interpolation errors. To improve the quality of demosaiced video sequences, we present a modified universal demosaicing scheme, which specifically recovers the G component in the color difference domain.

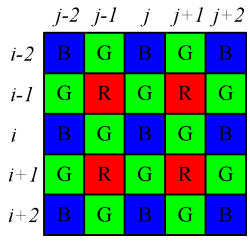

Fig. 2. 5×5 Bayer CFA mosaic subimage.

For a mosaic image frame F_M in a mosaic video sequence, denote by $F_M^K(i, j)$ the color value in channel K ($K \in \{R, G, B\}$) of the pixel at position (i, j) in F_M. To recover the missing K color component of a target pixel, the neighboring K color pixels in a window should be used. Denote by $\mathbb{W}^K(i, j)$ the set of positions of the K color pixels corresponding to a window centered at position (i, j). For illustration, considering a 5×5 Bayer CFA mosaic subimage shown in Fig. 2, we have $\mathbb{W}^G(i, j) = \{(i \pm 1, j), (i, j \pm 1)\}$ corresponding to a 3×3 window. Since adequate neighboring K color pixels are required to recover the missing K color component of the target pixel, the window size should be large enough that

$$|\mathbb{W}^K(i, j)| \geq T \tag{1}$$

where T represents a prespecified threshold and is set to be 3 empirically.

Since, in the proposed universal demosaicing scheme, G components will be used for recovering the R and B components, we first describe how to recover the missing G color components in the proposed scheme. Since the recovering of the missing G color components in the R color pixels is the same as that in the B color pixels, we only discuss how to recover the G color components in the B color pixels. When recovering the G color value for a B color pixel $F_M^B(i, j)$ in the mosaic image frame, the demosaiced G color value is the sum of its own B color value and the associated G-B color difference value, which is the weighted average of the G-B color difference values corresponding to the neighboring G color pixels in the window. That is, the demosaiced G color value of the pixel at position (i, j) can be calculated by

$$\hat{F}_{\mathrm{RGB}}^G(i, j) = F_M^B(i, j) + \frac{\sum_{(x,y)\in\mathbb{W}^G(i,j)} w_{\mathcal{D}_{\mathrm{GB}}}(x, y)\mathcal{D}_{\mathrm{GB}}(x, y)}{\sum_{(x,y)\in\mathbb{W}^G(i,j)} w_{\mathcal{D}_{\mathrm{GB}}}(x, y)} \tag{2}$$

where the G-B color difference value for each neighboring G pixel at position $(x, y) \in \mathbb{W}^G(i, j)$ is expressed as

$$\mathcal{D}_{\mathrm{GB}}(x, y) = F_M^G(x, y) - |\mathbb{W}^B(x, y)|^{-1} \sum_{(p,q)\in\mathbb{W}^B(x,y)} F_M^B(p, q) \tag{3}$$

and the associated weight is determined by

$$w_{\mathcal{D}_{\mathrm{GB}}}(x, y) = \left[1 + \sum_{(p,q)\in\mathbb{W}^G(i,j)} |\mathcal{D}_{\mathrm{GB}}(x, y) - \mathcal{D}_{\mathrm{GB}}(p, q)|\right]^{-1} \tag{4}$$

which incorporates the gradient information in the color difference domain. The rationale behind the weight is that the neighboring G pixel with very different G-B color difference value must lie in a nonhomogeneous region and should receive less weight in recovering the G pixel.

After recovering the missing G color components, to obtain the full color image frame, it is required to recover the missing R and B color components; the fully populated G color components can be utilized to assist in recovering the missing R and B color components. Since recovering the missing B color components in the R and G pixels is similar to recovering the missing R color components in the B and G pixels, we only specifically discuss the case of recovering the missing R color components in the B pixels.

For recovering the R color component in the B pixel at position (i, j), the demosaiced R color value is the sum of its own demosaiced G color value and the associated R-G color difference value, which is the weighted average of the R-G color difference values corresponding to the neighboring R color pixels at positions in $\mathbb{W}^R(i, j)$. That is, the demosaiced R color value can be calculated by

$$\hat{F}_{\mathrm{RGB}}^R(i, j) = \hat{F}_{\mathrm{RGB}}^G(i, j) + \frac{\sum_{(x,y)\in\mathbb{W}^R(i,j)} w_{\mathcal{D}_{\mathrm{RG}}}(x, y)\mathcal{D}_{\mathrm{RG}}(x, y)}{\sum_{(x,y)\in\mathbb{W}^R(i,j)} w_{\mathcal{D}_{\mathrm{RG}}}(x, y)} \tag{5}$$

where the R-G color difference value of the pixel at position (x, y) is expressed as $\mathcal{D}_{\mathrm{RG}}(x, y) = F_M^R(x, y) - \hat{F}_{\mathrm{RGB}}^G(x, y)$ and the associated weight is determined by $w_{\mathcal{D}_{\mathrm{RG}}}(x, y) = [1 + \sum_{(p,q)\in\mathbb{W}_N^R(i,j)} |\mathcal{D}_{\mathrm{RG}}(x, y) - \mathcal{D}_{\mathrm{RG}}(p, q)|]^{-1}$. Similarly, we can recover, in the color difference domain, the missing R components in the G pixels and the missing B color components in the R and G pixels. Note that the models for recovery and weight determination used in the above formulas follow those by Lukac and Plataniotis [23], [26], [27], [29] except that the G components are recovered and the associated weights are determined in the color difference domain. Once all the missing color components are recovered, the postprocessing step in [26] can be employed to further enhance the quality of the demosaiced video sequences.

Since the proposed universal demosaicing scheme recovers all the three color components in the color difference domain, the demosaiced video sequences using the proposed universal demosaicing scheme tend to have better quality for later H.264-based compression, implying better quality of the reconstructed video sequences after decompression.

III. Traditional Chroma Subsampling Strategy in H.264/AVC

In this section, we first describe the traditional chroma subsampling strategy in H.264/AVC and then point out the drawback at the decoder site. Given a mosaic image frame F_M, first demosaic F_M to obtain the full RGB color image frame $\hat{F}_{\mathrm{RGB}}$. Then, since the YUV color space is most commonly used in H.264/AVC, convert the image frame from RGB color space to YUV color space to obtain the YUV image frame F_{YUV}. The transforms between the RGB and YUV color

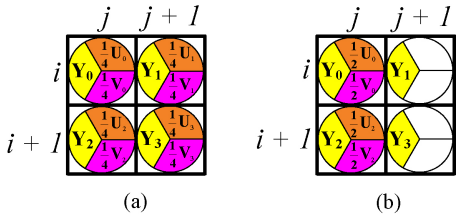

Fig. 3. Subsampling strategies with (a) 4:2:0(I) format and (b) 4:2:0(II) format in H.264/AVC.

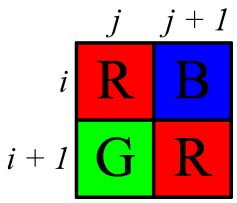

Fig. 4. 2×2 diagonal stripe CFA mosaic block.

spaces can be expressed [20] as

$$\begin{bmatrix} Y \\ U \\ V \end{bmatrix} = \begin{bmatrix} 0.257 & 0.504 & 0.098 \\ -0.148 & -0.291 & 0.439 \\ 0.439 & -0.368 & -0.071 \end{bmatrix} \begin{bmatrix} R \\ G \\ B \end{bmatrix} + \begin{bmatrix} 16 \\ 128 \\ 128 \end{bmatrix} \quad (6)$$

$$\begin{bmatrix} R \\ G \\ B \end{bmatrix} = \begin{bmatrix} 1.164 & 0 & 1.596 \\ 1.164 & -0.391 & -0.813 \\ 1.164 & 2.018 & 0 \end{bmatrix} \begin{bmatrix} Y - 16 \\ U - 128 \\ V - 128 \end{bmatrix}. \quad (7)$$

To compress the YUV image frame by H.264 video coder, for each 2×2 block, all four Y components are retained but only one U and one V components are calculated according to some subsampling strategy. The subsampling strategy with format 4:2:0(I) shown in Fig. 3(a) determines the U component associated with the block as the average of all four U components in the block. The V component associated with the block is determined similarly. The subsampling strategy with format 4:2:0(II), shown in Fig. 3(b), determines the U and V components associated with the block as the average of the two U and V components in the left column of the block, respectively.

Now we point out the drawback of the traditional chroma subsampling strategy at the decoder site. According to (7), it is clear that only the Y and V components are required to reconstruct the R pixel, implying that the V component is more significant than the U component when reconstructing the R pixel. Similarly, the U component is more significant than the V component when reconstructing the B pixel. The traditional chroma subsampling strategy ignores these facts and always samples the U and V chroma components by the same way, resulting in quality degradation in the reconstructed mosaic video sequences. To alleviate this problem, Chen *et al.* [4] proposed a chroma subsampling strategy specifically for the mosaic video sequences with the Bayer CFA structure. However, Chen *et al.*'s strategy cannot be used for the mosaic video sequences with non-Bayer CFA structures. Thus, in the next section, for the arbitrary RGB-CFAs, we propose a modified universal chroma subsampling strategy, which considers the significance of the U and V components when reconstructing the R and B pixels.

IV. Proposed Universal Chroma Subsampling Strategy

Denote by $\mathbb{B}^K(i, j)$ the set of positions of the $K (K \in \{R, G, B\})$ color pixels in the 2×2 mosaic block with the upper-left corner pixel positioned at (i, j). For illustration, considering the 2×2 diagonal stripe CFA mosaic block shown in Fig. 4, we have $\mathbb{B}^R(i, j) = \{(i, j), (i + 1, j + 1)\}$. Let F_{YUV} represent a YUV image frame, obtained by demosaicing and color space converting processes, and denote by $F^L_{\text{YUV}}(i, j)$ the value of component L ($L \in \{Y, U, V\}$) of the pixel at position (i, j) in F_{YUV}.

For each 2×2 block in F_{YUV}, retain four Y components and sample the U and V components by the chroma subsampling strategy. According to the corresponding CFA structure, the proposed universal chroma subsampling strategy selects the proper pixels to sample the U and V chroma components by considering the significance of the U and V components for reconstructing R and B pixels. Since, when reconstructing the R pixels at the decoder site, V components are more significant than U components, the sampled V component associated with the block, when encoding, is determined as the average of the V components corresponding to the R pixels in the block. Similarly, the sampled U component associated with the block, when encoding, is determined as the average of the U components corresponding to the B pixels in the block. For a 2×2 YUV block with an upper-left corner pixel positioned at (i, j), the sampled U and V components associated with the B and R pixels, respectively, are determined by

$$\begin{aligned} U_B(i, j) &= |\mathbb{B}^B(i, j)|^{-1} \sum_{(x,y)\in\mathbb{B}^B(i,j)} F^U_{\text{YUV}}(x, y) \\ V_R(i, j) &= |\mathbb{B}^R(i, j)|^{-1} \sum_{(x,y)\in\mathbb{B}^R(i,j)} F^V_{\text{YUV}}(x, y) \end{aligned} \quad (8)$$

for the cases of $|\mathbb{B}^B(i, j)| > 0$ and $|\mathbb{B}^R(i, j)| > 0$. As for the case of $\mathbb{B}^B(i, j) = \emptyset$, we use the traditional subsampling strategy with format 4:2:0(I) to determine the subsampled U component of the block. The same strategy is used to deal with the case where $\mathbb{B}^R(i, j) = \emptyset$. Since the proposed universal subsampling strategy considers the significance of the U and V components in decoding, the proposed method can achieve better quality of the reconstructed mosaic video sequences. The subsampled YUV image frame is then compressed by the H.264 encoder. One specific thing to be noted is that, for the case of the Bayer CFA, the sampling result of the proposed universal subsampling strategy is the same as that of Chen *et al.*'s subsampling strategy [4], an efficient subsampling strategy for Bayer CFA video sequences.

After compressing the mosaic video sequences, the reconstruction of the video sequence at the decoder site can be described as follows. For each reconstructed 2×2 block in an image frame, we have four reconstructed Y components corresponding to the four pixels, one reconstructed U, and one

reconstructed V component. Thus, we can reconstruct each R pixel by the reconstructed V component and its own Y component. Similarly, each B pixel is reconstructed using the reconstructed U component and its own Y component. As for reconstructing the G pixel, all Y, U, and V components are required. The required U component is interpolated from the reconstructed U components of the three nearest neighboring B pixels and the required V component from the three nearest neighboring R pixels. When there exist no B pixels in the block, meaning that the traditional subsampling strategy is used to determine the sampled U component, the traditional reconstruction approach is used to reconstruct the U component. Similarly, when there exist no R pixels in the block, the traditional reconstruction approach is used to reconstruct the V component.

We now describe the detailed steps of the compression and reconstruction processes for each input mosaic image frame with arbitrary CFA structures. Given a mosaic image frame F_M, the compression process involves five steps.

Step 1) Obtain, from the video header, the mosaic structure.
Step 2) Demosaic F_M to obtain the demosaiced image frame $\hat{F}_{\mathrm{RGB}}$ by the demosaicing scheme in Section II.
Step 3) Obtain the YUV image frame F_{YUV} by converting each pixel in $\hat{F}_{\mathrm{RGB}}$ to the YUV color space.
Step 4) Obtain the subsampled YUV image frame F'_{YUV} by sampling the U and V components for each 2×2 block in F_{YUV}.
Step 5) Encode, using the H.264 encoder, F'_{YUV} to obtain the compressed bit stream.

Given an input compressed bit stream, the reconstruction process involves three steps.

Step 1) Recover the video header and obtain the mosaic structure.
Step 2) Reconstruct the subsampled YUV image frame $\tilde{F}'_{\mathrm{YUV}}$ by decoding, using the H.264 decoder, the input compressed bit stream.
Step 3) Obtain the mosaic image frame $\tilde{F}_M$ by reconstructing the R, G, and B pixels for each 2×2 block in $\tilde{F}'_{\mathrm{YUV}}$.

In addition to the single-color RGB-CFAs, the proposed universal method can also be used to tackle two color RGB-CFAs, such as the DTDI CFA, when we only consider one missing color in the demosaicing step. For the case of DTDI CFA, the proposed universal compression and reconstruction processes yield almost the same results as the previous method in [10].

V. Experimental Results

For comparison, the proposed universal chroma subsampling strategy was compared with the traditional chroma subsampling strategy in H.264/AVC. The experiments were conducted on the six test video sequences shown in Fig. 5, which were adopted from [39]. For each video sequence, the number of frames is 200 and the spatial resolution for each image frame is 352×288. The four test video sequences were first downsampled to obtain the mosaic video sequences with seven RGB-CFA structures shown in Fig. 1. Then, we performed the compression and reconstruction processes with the traditional and the proposed universal chroma subsampling strategies on the mosaic video sequences. As for the universal demosaicing scheme, Lukac and Plataniotis' scheme and the proposed scheme were used, where the postprocessing step in [26] was applied to refine the demosaiced video quality. The group of pictures consisted of one intraframe and nine interframes. In addition, the seven different quantization parameters (QPs) considered in the compression process were 8, 12, 16, 20, 24, 28, and 32. All the experiments were implemented on the IBM compatible computer with Intel Core i7-960 CPU of 3.2 GHz, 24 GB RAM, and Microsoft Windows 7 64-bit operating system. The demosaicing and subsampling schemes were implemented in Borland C++ Builder 6.0. The compression platform was JM17.2 [40], which was realized in Visual C++ 2008. Furthermore, all the experimental results can be found in [39].

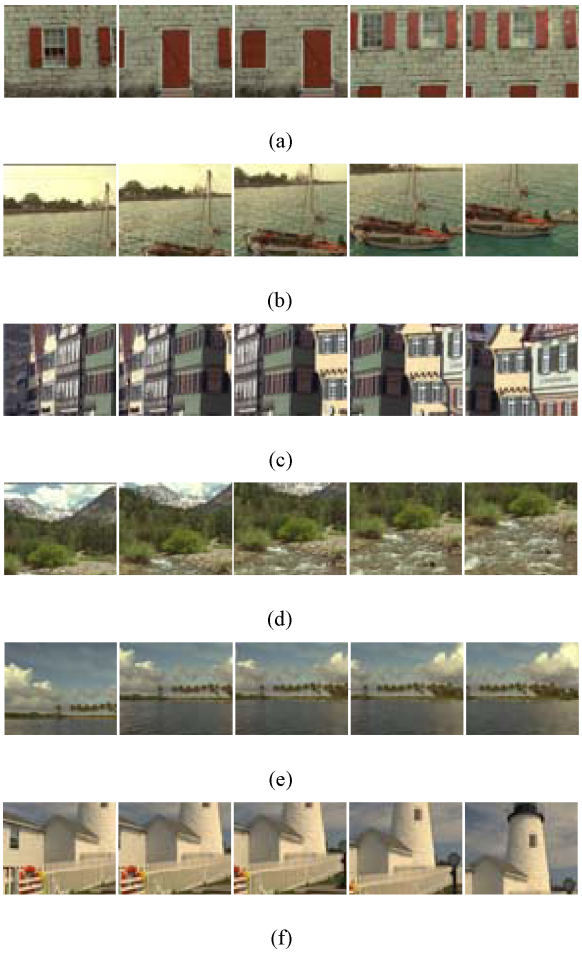

Fig. 5. Test video sequences. (a) *Wall*. (b) *Boat*. (c) *Houses*. (d) *Nature*. (e) *Island*. (f) *Lighthouse*.

A. Comparison of the Demosaicing Schemes

Since the proposed universal demosaicing scheme recovers G color values in the color difference domain, instead of the spatial domain, we first compared the demosaicing performance with Lukac and Plataniotis' demosaicing scheme. The objective comparisons were based on two color video sequence quality performance measures: the color peak signal-to-noise ratio (CPSNR) and the S-CIELAB ΔE^*_{ab}. Let $\Psi = \{R, G, B\}$

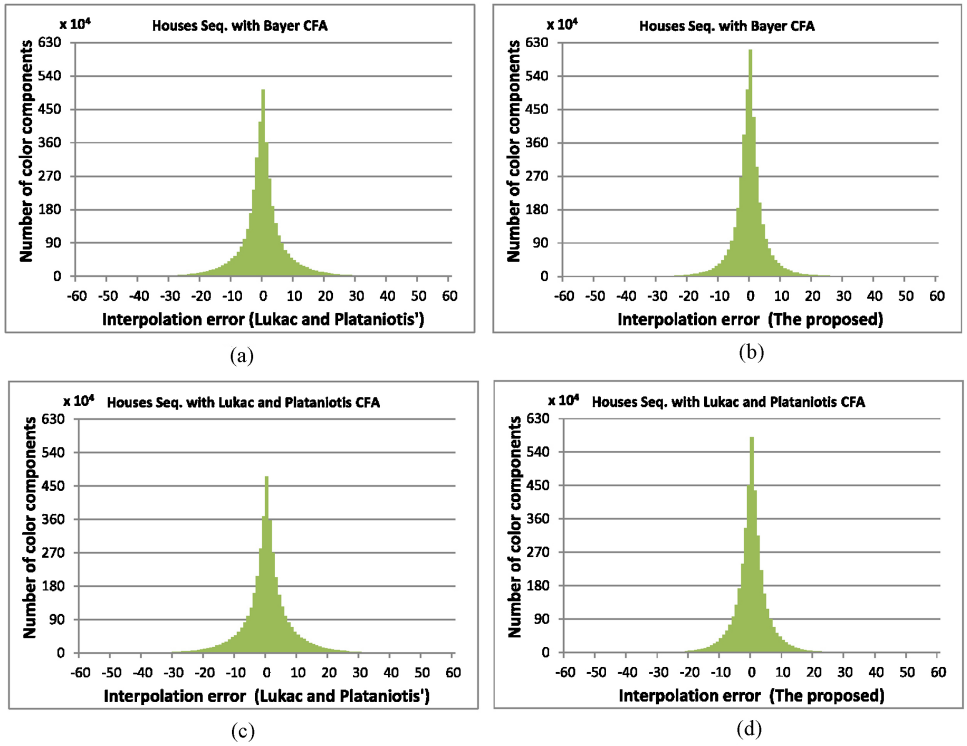

Fig. 6. Interpolation error histograms based on the *Houses* sequence. (a) Lukac and Plataniotis' scheme for the Bayer CFA structure. (b) Proposed scheme for the Bayer CFA structure. (c) Lukac and Plataniotis' scheme for the Lukac and Plataniotis CFA structure. (d) Proposed scheme for the Lukac and Plataniotis CFA structure.

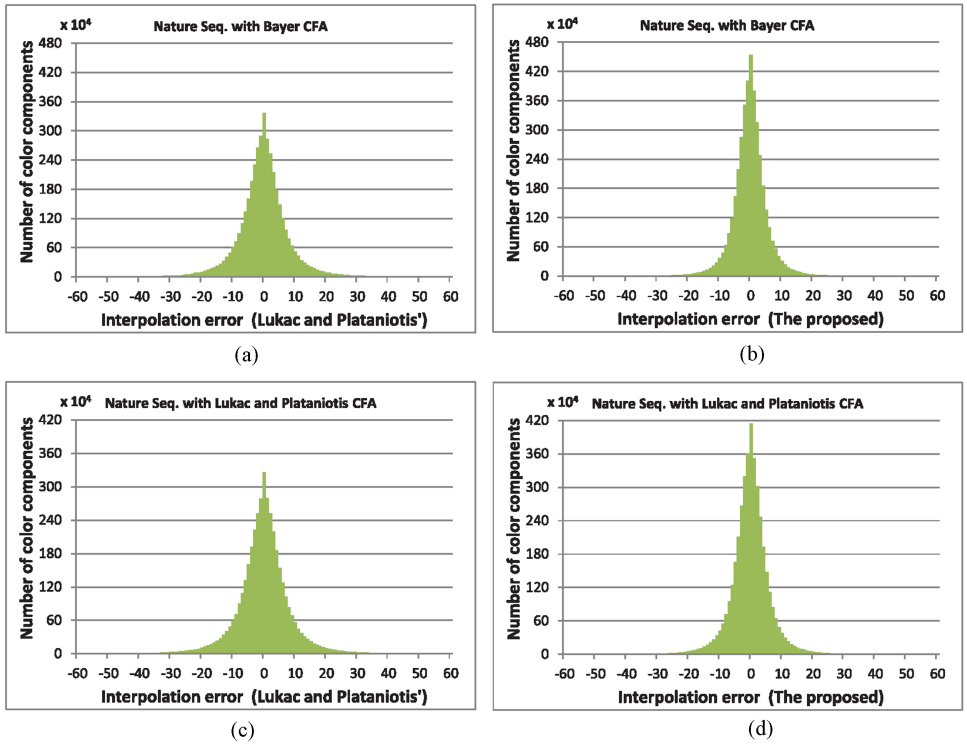

Fig. 7. Interpolation error histograms based on the *Nature* sequence. (a) Lukac and Plataniotis' scheme for the Bayer CFA structure. (b) Proposed scheme for the Bayer CFA structure. (c) Lukac and Plataniotis' scheme for the Lukac and Plataniotis CFA structure. (d) Proposed scheme for the Lukac and Plataniotis CFA structure.

TABLE I

CPSNR VALUES OF THE DEMOSAICED VIDEO SEQUENCES BY LUKAC AND PLATANIOTIS' AND THE PROPOSED UNIVERSAL SCHEMES

	Bayer CFA		Lukac and Plataniotis CFA		Yamanaka CFA	
Video Sequence	Lukac and Plataniotis'	Proposed	Lukac and Plataniotis'	Proposed	Lukac and Plataniotis'	Proposed
Wall	35.70	38.23	30.85	31.45	25.81	25.95
Boat	34.36	36.45	30.13	30.60	26.28	26.46
Houses	32.72	34.81	28.99	29.46	19.75	19.87
Nature	32.97	34.76	28.36	28.86	25.76	26.13
Island	39.91	41.51	34.12	34.47	30.14	30.24
Lighthouse	35.63	37.50	30.72	31.23	22.52	22.56
	Diagonal Stripe CFA		Vertical Stripe CFA		Modified Bayer CFA	
Video Sequence	Lukac and Plataniotis'	Proposed	Lukac and Plataniotis'	Proposed	Lukac and Plataniotis'	Proposed
Wall	35.05	37.59	34.32	36.47	31.97	33.20
Boat	34.31	36.22	33.31	35.16	32.20	33.40
Houses	29.97	31.76	33.10	34.79	32.98	34.50
Nature	32.13	34.21	32.20	33.92	28.03	28.99
Island	40.14	41.44	38.70	40.21	37.27	38.35
Lighthouse	33.25	34.76	36.36	37.76	34.23	35.74
	HVS-Based CFA		Average			
Video Sequence	Lukac and Plataniotis'	Proposed	Lukac and Plataniotis'	Proposed		
Wall	33.93	35.64	32.96	34.08		
Boat	33.90	35.42	32.37	33.39		
Houses	33.71	34.87	29.74	31.44		
Nature	29.96	31.52	30.50	31.20		
Island	39.32	40.33	37.50	38.08		
Lighthouse	35.73	36.71	32.49	33.75		

TABLE II

S-CIELAB ΔE^*_{ab} VALUES OF THE DEMOSAICED VIDEO SEQUENCES BY LUKAC AND PLATANIOTIS' AND THE PROPOSED UNIVERSAL SCHEMES

	Bayer CFA		Lukac and Plataniotis CFA		Yamanaka CFA	
Video Sequence	Lukac and Plataniotis'	Proposed	Lukac and Plataniotis'	Proposed	Lukac and Plataniotis'	Proposed
Wall	2.2637	1.4769	2.6355	1.7873	2.3071	1.7339
Boat	2.4200	1.6493	2.7979	1.9558	2.2646	1.7840
Houses	2.8170	1.9326	3.1259	2.1228	3.8453	3.0658
Nature	3.4527	2.4452	3.6538	2.7768	3.4426	2.7721
Island	1.3306	1.0276	1.5020	1.1622	1.1695	1.0261
Lighthouse	1.6541	1.1772	1.7304	1.2714	2.1302	1.7359
	Diagonal Stripe CFA		Vertical Stripe CFA		Modified Bayer CFA	
Video Sequence	Lukac and Plataniotis'	Proposed	Lukac and Plataniotis'	Proposed	Lukac and Plataniotis'	Proposed
Wall	2.5021	2.0895	5.2020	4.9819	2.7620	2.3497
Boat	2.3348	1.9561	4.5196	4.3177	2.5740	2.1990
Houses	2.5079	2.1219	9.8962	9.6977	2.5357	2.0572
Nature	4.0627	3.5106	6.8469	6.5480	4.6104	4.1373
Island	1.2734	1.1754	2.3774	2.3115	1.4574	1.3196
Lighthouse	1.6557	1.4700	5.7695	5.6921	1.8013	1.5122
	HVS-Based CFA		Average			
Video Sequence	Lukac and Plataniotis'	Proposed	Lukac and Plataniotis'	Proposed		
Wall	3.1827	2.7443	2.9793	2.4519		
Boat	3.2934	2.9025	2.8863	2.3949		
Houses	3.8081	3.1909	4.0766	3.4556		
Nature	4.6613	4.1660	4.3900	3.7651		
Island	1.8103	1.6479	1.5601	1.3815		
Lighthouse	2.4155	2.0916	2.4510	2.1358		

denote the set of RGB color components. The CPSNR of a demosaiced video sequence with N image frames of size $X \times Y$ can be expressed as

$$\text{CPSNR} = 10 \log_{10} \frac{255^2}{\frac{1}{N}\sum_{n=1}^{N} \text{CMSE}^n} \tag{9}$$

with

$$\text{CMSE}^n = \frac{1}{3XY} \sum_{i=0}^{X-1} \sum_{j=0}^{Y-1} \sum_{K \in \Psi} \left[F^{K,n}_{\text{RGB}}(i, j) - \hat{F}^{K,n}_{\text{RGB}}(i, j) \right]^2 \tag{10}$$

where $F^{K,n}_{\text{RGB}}(i, j)$ and $\hat{F}^{K,n}_{\text{RGB}}(i, j)$ denote the K ($K \in \Psi$) color value of the pixel at position (i, j) in the nth image frame of the original and demosaiced video sequences, respectively. Higher values of the CPSNR indicate better quality of the demosaiced video sequences. Let $\Phi = \{L, a, b\}$ denote the set of CIELAB color components. The S-CIELAB ΔE^*_{ab} of a demosaiced video sequence with N image frames of size $X \times Y$ is defined as

$$\Delta E^*_{ab} = \sum_{n=1}^{N} \sum_{i=0}^{X-1} \sum_{j=0}^{Y-1} \left\{ \sum_{C \in \Phi} \left[F^{C,n}_{\text{LAB}}(i, j) - \hat{F}^{C,n}_{\text{LAB}}(i, j) \right]^2 \right\}^{\frac{1}{2}} \tag{11}$$

(a) (b) (c)

Fig. 8. Based on the *Houses* video sequence with Lukac and Plataniotis CFA structure. (a) Magnified subimages of the original image frame. Corresponding demosaiced subimages generated by (b) Lukac and Plataniotis' demosaicing schemes and (c) the proposed scheme.

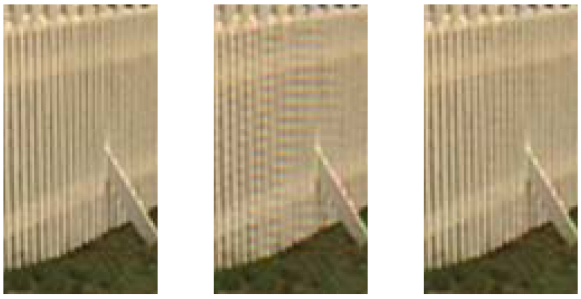

(a) (b) (c)

Fig. 9. Based on the *Lighthouse* video sequence with modified Bayer CFA structure. (a) Magnified subimages of the original image frame. Corresponding demosaiced subimages generated by (b) Lukac and Plataniotis' demosaicing schemes and (c) the proposed scheme.

where $F_{\mathrm{LAB}}^{C,n}(i,j)$ and $\hat{F}_{\mathrm{LAB}}^{C,n}(i,j)$ denote the C ($C \in \Phi$) CIELAB color value of the pixel at position (i,j) in the nth image frame of the original and demosaiced video sequences, respectively. The transformation between the RGB color space and the CIELAB color space is referred to in [18]. Lower values of the ΔE_{ab}^{*} indicate better quality of the demosaiced video sequences. Based on the six test video sequences with seven RGB-CFA structures, Tables I and II give the comparison results in terms of the CPSNR and ΔE_{ab}^{*} values, respectively. It is evident that the proposed universal demosaicing scheme delivered significantly better quality of the demosaiced video sequences when compared with Lukac and Plataniotis' scheme.

In addition to evaluating the average interpolation errors at the video sequence level, such as CPSNR, evaluating the interpolation errors at the pixel level is also important and should be addressed. Specifically, the *Houses* and *Nature* video sequences with a lot of edges and fine details were used to illustrate the comparison results with respect to the interpolation errors at the pixel level. Based on the *Houses* video sequence with the Bayer CFA structure and the Lukac and Plataniotis CFA structure, Fig. 6 shows the histograms of the interpolation errors corresponding to Lukac and Plataniotis' scheme and the proposed scheme. Clearly, the proposed scheme generates sharper Laplacian distributions of the interpolation errors, indicating that the proposed universal demosaicing scheme achieved better quality of the demosaiced video sequences. Similar comparison results for the *Nature* video sequence are shown in Fig. 7.

Apart from the objective metrics, a subjective visual evaluation was used to demonstrate the effectiveness of the proposed universal demosaicing scheme on the edge regions. Image frames with detailed textures taken from the *Houses* and *Lighthouse* video sequences were used for evaluation. Demosaicing often generates color artifacts on texture regions and results in unpleasing visual perception. For the *Houses* video sequence, Fig. 8(a)–(c) shows the magnified subimages of the original image frame and the corresponding demosaiced subimages generated by Lukac and Plataniotis' proposed schemes, respectively. It is clear that the proposed demosaicing scheme produced fewer color artifacts than Lukac and Plataniotis' demosaicing scheme. The image frame from the *Lighthouse* video sequence tends to generate color artifacts after demosaicing. For the *Lighthouse* video sequence, Fig. 9(a)–(c) gives the magnified subimages of the original image frame and the corresponding demosaiced subimages generated by Lukac and Plataniotis' scheme and the proposed schemes, respectively. It is observed that the proposed demosaicing scheme has significantly better visual effect.

B. Comparison of the Chroma Subsampling Strategies

Next, we compared the proposed universal chroma subsampling strategy with the traditional chroma subsampling strategy based on the quality of the reconstructed mosaic video sequences. The PSNR measures the quality of the reconstructed mosaic video sequences whereas the bitrate represents the compression performance. We compared the quality of the reconstructed mosaic video sequences by calculating the PSNR for each reconstructed mosaic video sequence for different values of bitrate determined by common values of QP. The PSNR of a reconstructed mosaic video sequence with N image frames of size $X \times Y$ can be expressed as

$$\mathrm{PSNR} = 10\log_{10}\frac{255^2}{\frac{1}{NXY}\sum_{n=1}^{N}\sum_{i=0}^{X-1}\sum_{j=0}^{Y-1}\left[F_M^n(i,j)-\hat{F}_M^n(i,j)\right]^2} \tag{12}$$

where $F_M^n(i,j)$ and $\hat{F}_M^n(i,j)$ denote the color value of the pixel at position (i,j) in the nth image frame of the original and reconstructed mosaic video sequences, respectively. Higher values of the PSNR indicate better quality of the reconstructed mosaic video sequences. The bitrate of a reconstructed mosaic video sequence $\hat{V}_M$ with H frames per second is defined as

$$\mathrm{bitrate} = \frac{N_b(\hat{V}_M)}{\frac{1}{H}N_f(\hat{V}_M)} \tag{13}$$

where $N_b(\hat{V}_M)$ and $N_f(\hat{V}_M)$ represents the bit number and the frame number of the mosaic video sequence, respectively. Lower values of the bitrate indicate better compression performance.

Figs. 10–16 depict the PSNR against different values of bitrate for different combinations of universal demosaicing schemes and subsampling strategies. The red and blue rate-distortion (RD) curves denote the results using

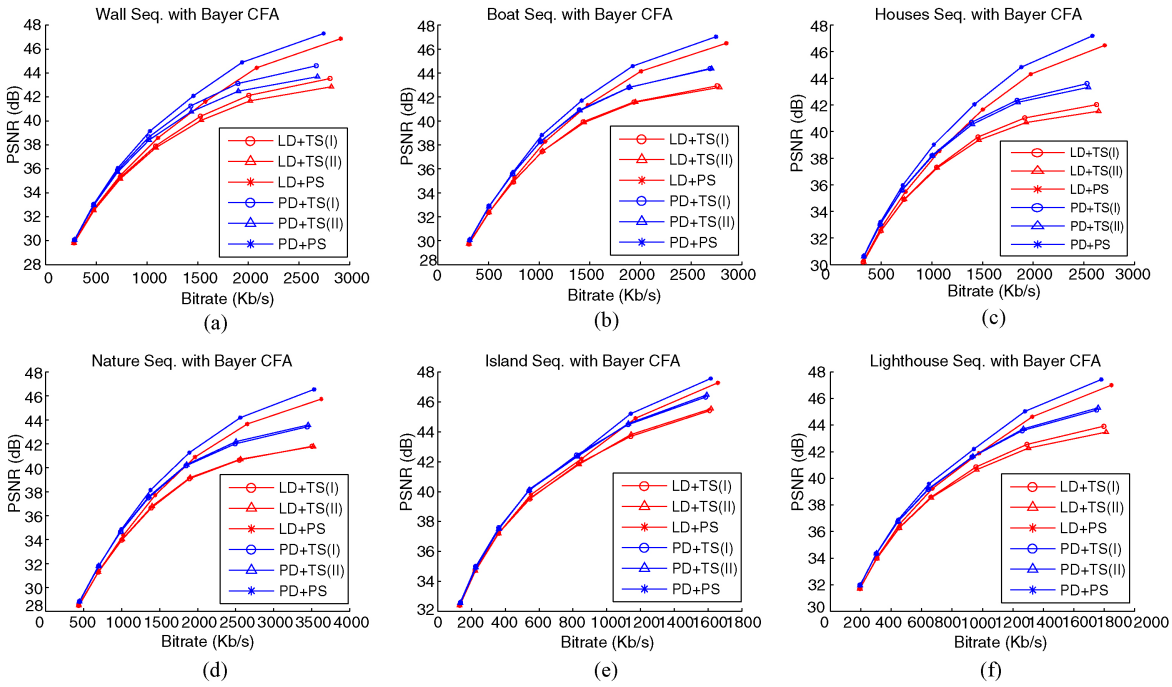

Fig. 10. PSNR against bitrate for different combinations of demosaicing schemes and subsampling strategies for video sequences under the Bayer CFA. (a) *Wall*. (b) *Boat*. (c) *Houses*. (d) *Nature*. (e) *Island*. (f) *Lighthouse*.

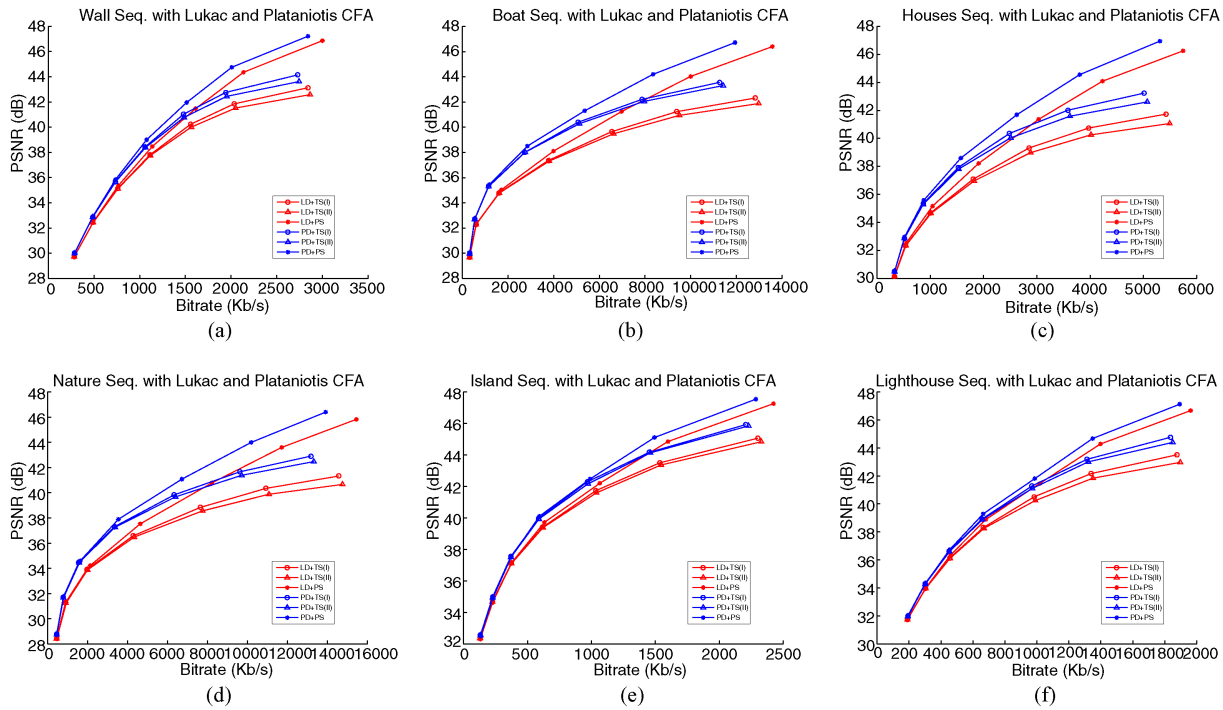

Fig. 11. PSNR against bitrate for different combinations of demosaicing schemes and subsampling strategies for video sequences under the Lukac and Plataniotis CFA. (a) *Wall*. (b) *Boat*. (c) *Houses*. (d) *Nature*. (e) *Island*. (f) *Lighthouse*.

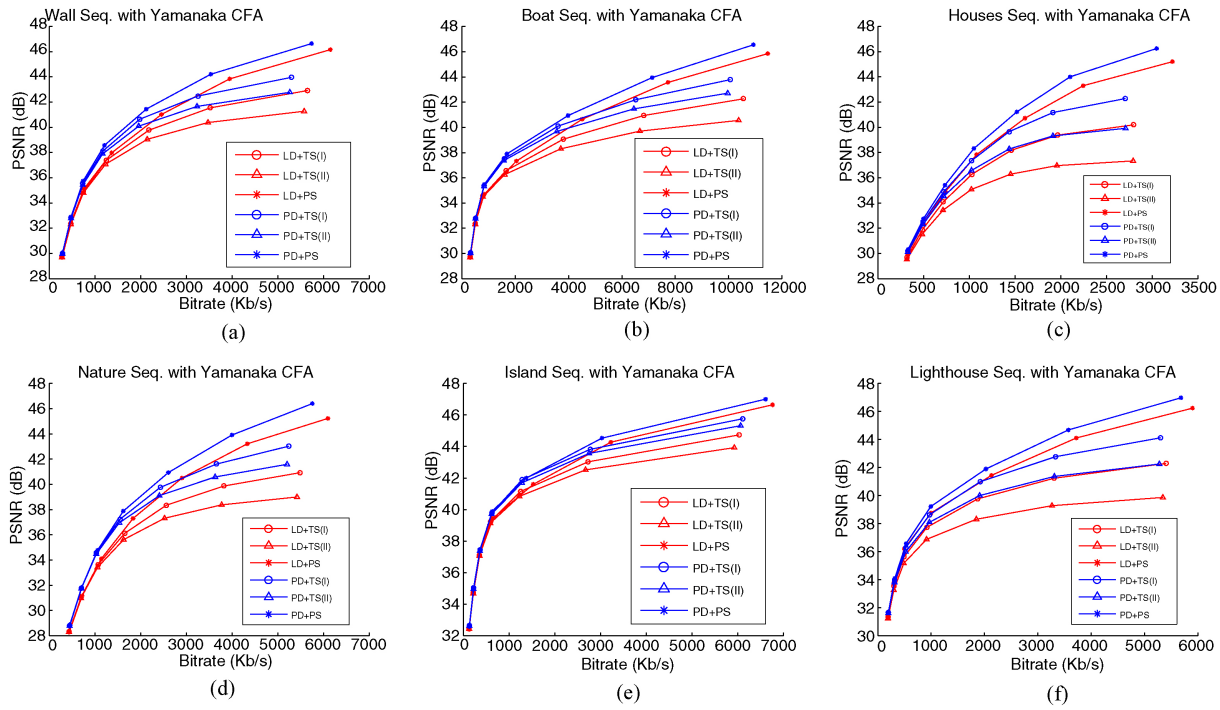

Fig. 12. PSNR against bitrate for different combinations of demosaicing schemes and subsampling strategies for video sequences under the Yamanaka CFA. (a) *Wall*. (b) *Boat*. (c) *Houses*. (d) *Nature*. (e) *Island*. (f) *Lighthouse*.

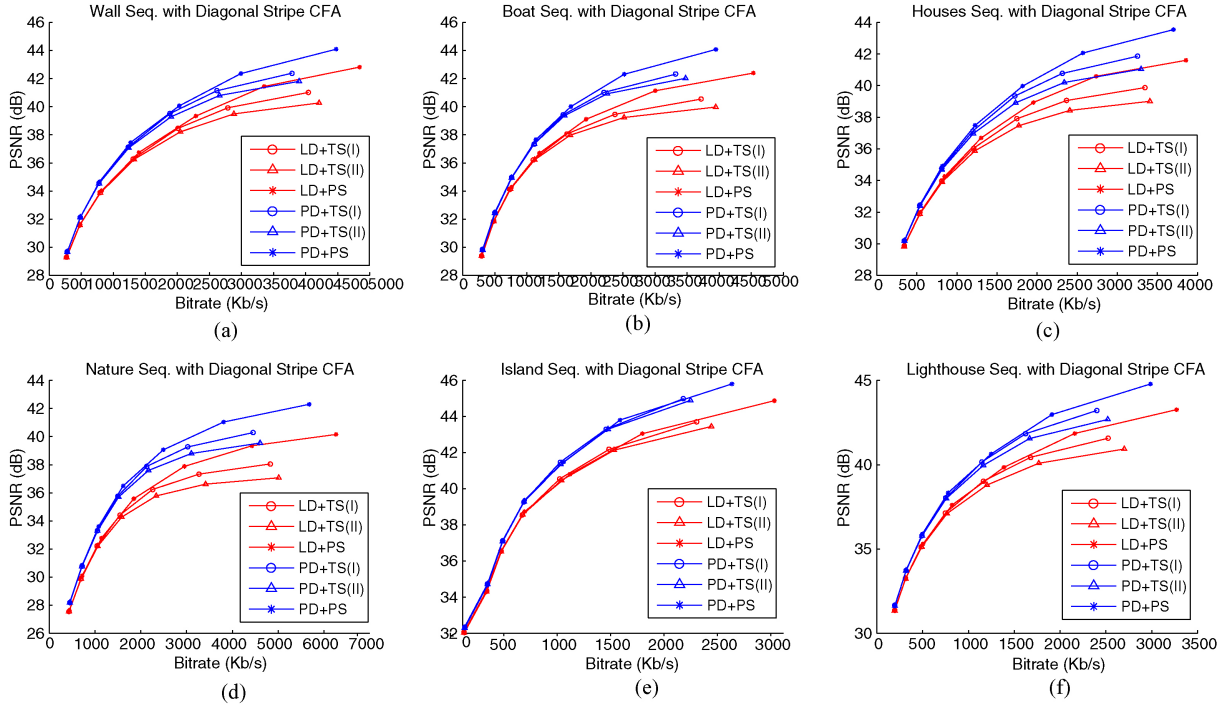

Fig. 13. PSNR against bitrate for different combinations of demosaicing schemes and subsampling strategies for video sequences diagonal stripe CFA. (a) *Wall*. (b) *Boat*. (c) *Houses*. (d) *Nature*. (e) *Island*. (f) *Lighthouse*.

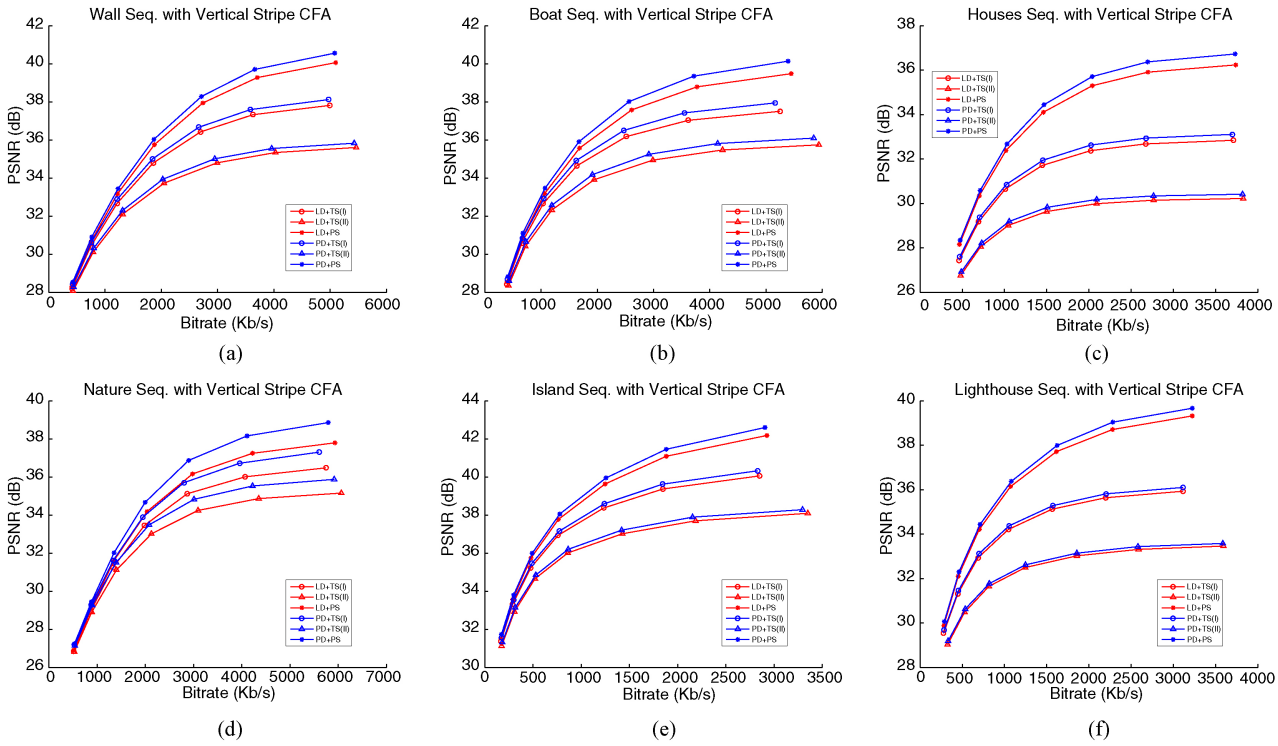

Fig. 14. Under the vertical stripe CFA, PSNR against bitrate for different combinations of demosaicing schemes and subsampling strategies for video sequences. (a) *Wall*. (b) *Boat*. (c) *Houses*. (d) *Nature*. (e) *Island*. (f) *Lighthouse*.

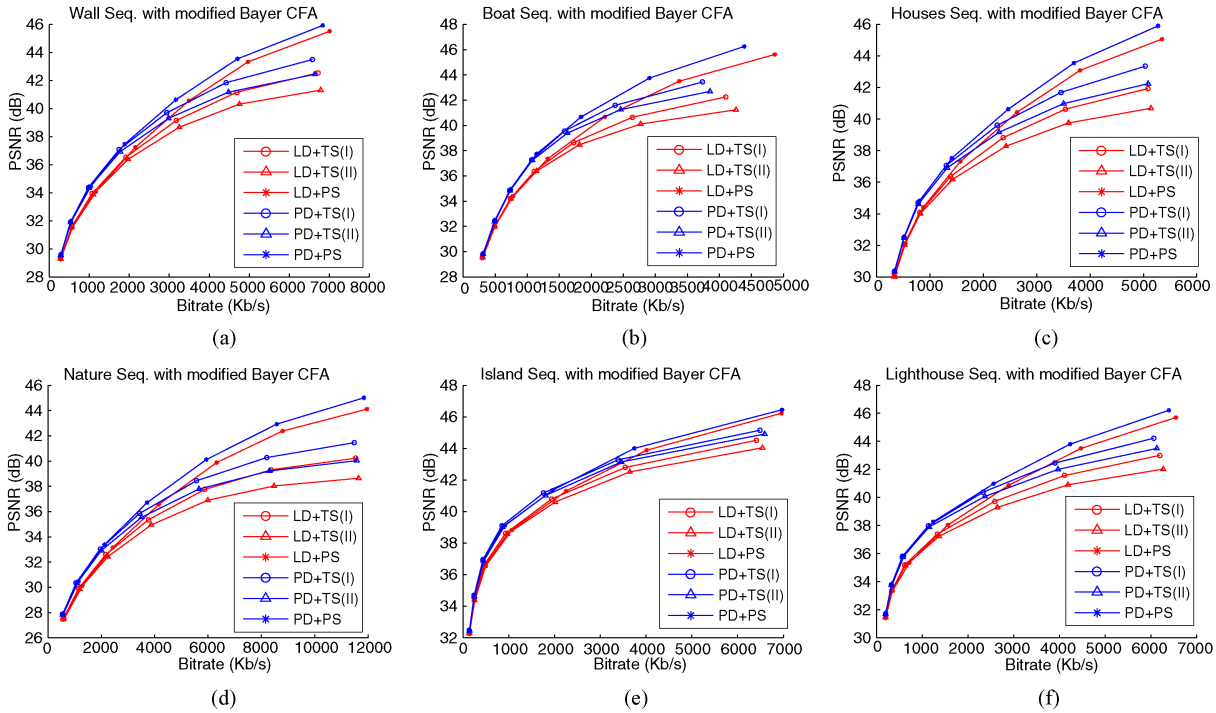

Fig. 15. PSNR against bitrate for different combinations of demosaicing schemes and subsampling strategies for video sequences under the modified Bayer CFA. (a) *Wall*. (b) *Boat*. (c) *Houses*. (d) *Nature*. (e) *Island*. (f) *Lighthouse*.

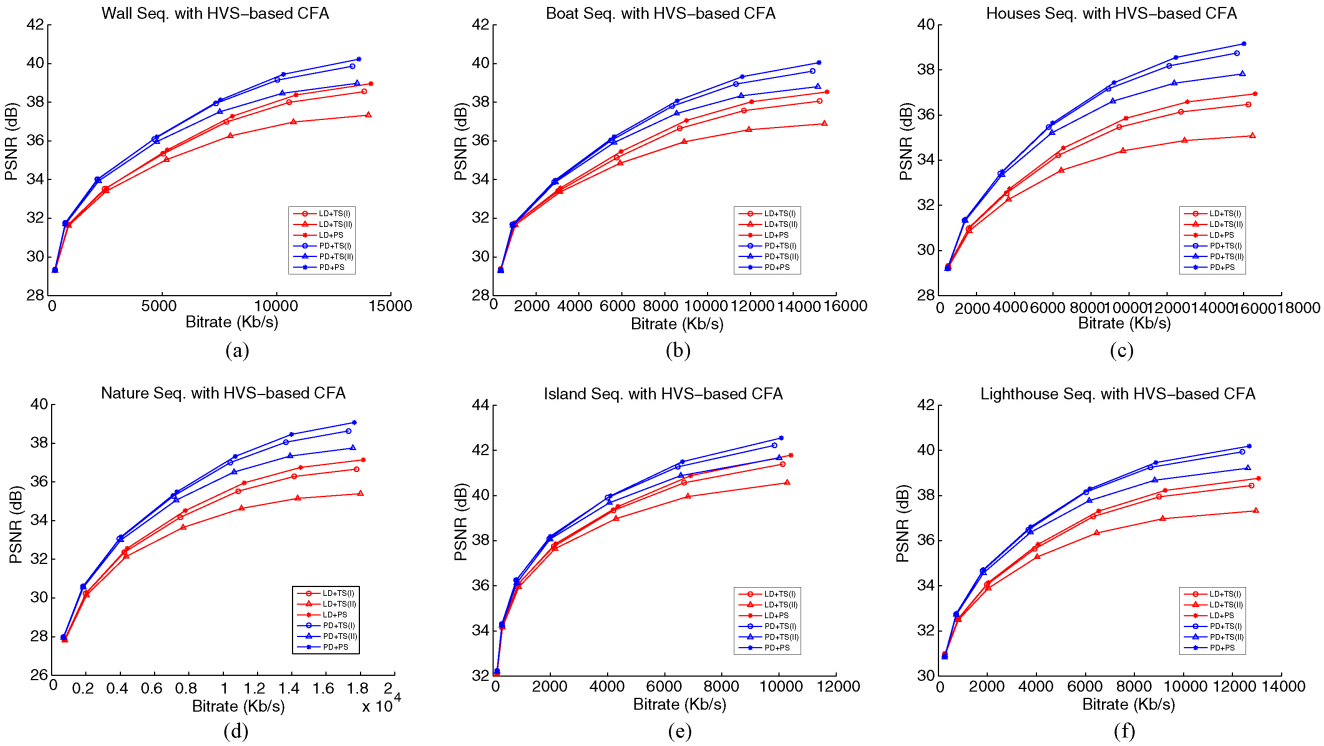

Fig. 16. PSNR against bitrate for different combinations of demosaicing schemes and subsampling strategies for video sequences under the HVS-based CFA. (a) *Wall*. (b) *Boat*. (c) *Houses*. (d) *Nature*. (e) *Island*. (f) *Lighthouse*.

TABLE III

GAIN, MEASURED BY BD-PSNR (DB) AND BD-BR (%), OF THE PROPOSED CHROMA SUBSAMPLING STRATEGY OVER THE TWO TRADITIONAL SUBSAMPLING STRATEGIES

		Demosaicing Method: LD				Demosaicing Method: PD			
		TS(I)		TS(II)		TS(I)		TS(II)	
Video Sequence	QP	BD-PSNR	BD-BR	BD-PSNR	BD-BR	BD-PSNR	BD-BR	BD-PSNR	BD-BR
Wall	8–20	1.1198	15.3583	1.9817	26.8340	0.8663	17.1556	1.5248	29.6076
	12–24	0.5289	8.5576	1.0880	17.4403	0.4383	10.2315	0.8688	19.8445
	16–30	0.2189	4.4328	0.5653	11.1175	0.2076	5.8748	0.4788	12.9619
	20–32	0.0779	1.7266	0.2784	6.3663	0.0890	2.7052	0.2495	7.5519
Boat	8–20	1.2218	19.5380	1.9073	29.8152	0.8442	19.6264	1.2863	29.4518
	12–24	0.6129	11.6219	1.0402	19.3036	0.4443	12.1097	0.7330	19.5071
	16–30	0.2575	6.1099	0.5152	11.8130	0.1971	6.3914	0.3818	11.8770
	20–32	0.0815	1.8845	0.2452	6.0858	0.0666	2.0602	0.1926	6.2293
Houses	8–20	1.8394	27.0576	2.9831	44.6314	1.3000	26.5863	2.1292	42.9355
	12–24	1.1516	19.0913	1.9982	32.4968	0.8020	18.8700	1.4106	32.3090
	16–30	0.6755	13.5474	1.2621	24.5208	0.4835	13.6775	0.9084	24.6718
	20–32	0.3757	8.9617	0.7557	17.6484	0.2864	9.3612	0.5684	18.1282
Nature	8–20	1.4935	21.3627	2.2996	32.6226	1.0519	20.7096	1.5617	30.0854
	12–24	0.8022	12.5273	1.3208	20.0668	0.5574	11.9913	0.8713	18.1045
	16–30	0.3404	6.0838	0.6482	11.2366	0.2366	5.7849	0.4156	9.7716
	20–32	0.0710	1.3168	0.2342	4.7043	0.0557	1.4293	0.1513	4.0768
Island	8–20	0.5209	11.7887	1.0190	22.7644	0.3788	13.0094	0.7296	25.0763
	12–24	0.2143	5.5304	0.5661	14.7824	0.1634	6.3530	0.4305	16.7194
	16–30	0.0781	2.1620	0.3259	8.8820	0.0657	2.5938	0.2622	10.2017
	20–32	0.0038	0.1356	0.1723	4.6825	0.0008	0.0107	0.1441	5.4834
Lighthouse	8–20	1.2486	22.6158	2.2277	39.3837	0.8838	23.3327	1.5278	39.1902
	12–24	0.7261	15.6010	1.4426	30.1340	0.5314	16.9177	1.0169	31.2094
	16–30	0.4138	10.4532	0.9315	22.3003	0.3189	11.6128	0.6791	23.3262
	20–32	0.2179	5.9793	0.5787	15.3556	0.1728	6.5956	0.4343	16.0493

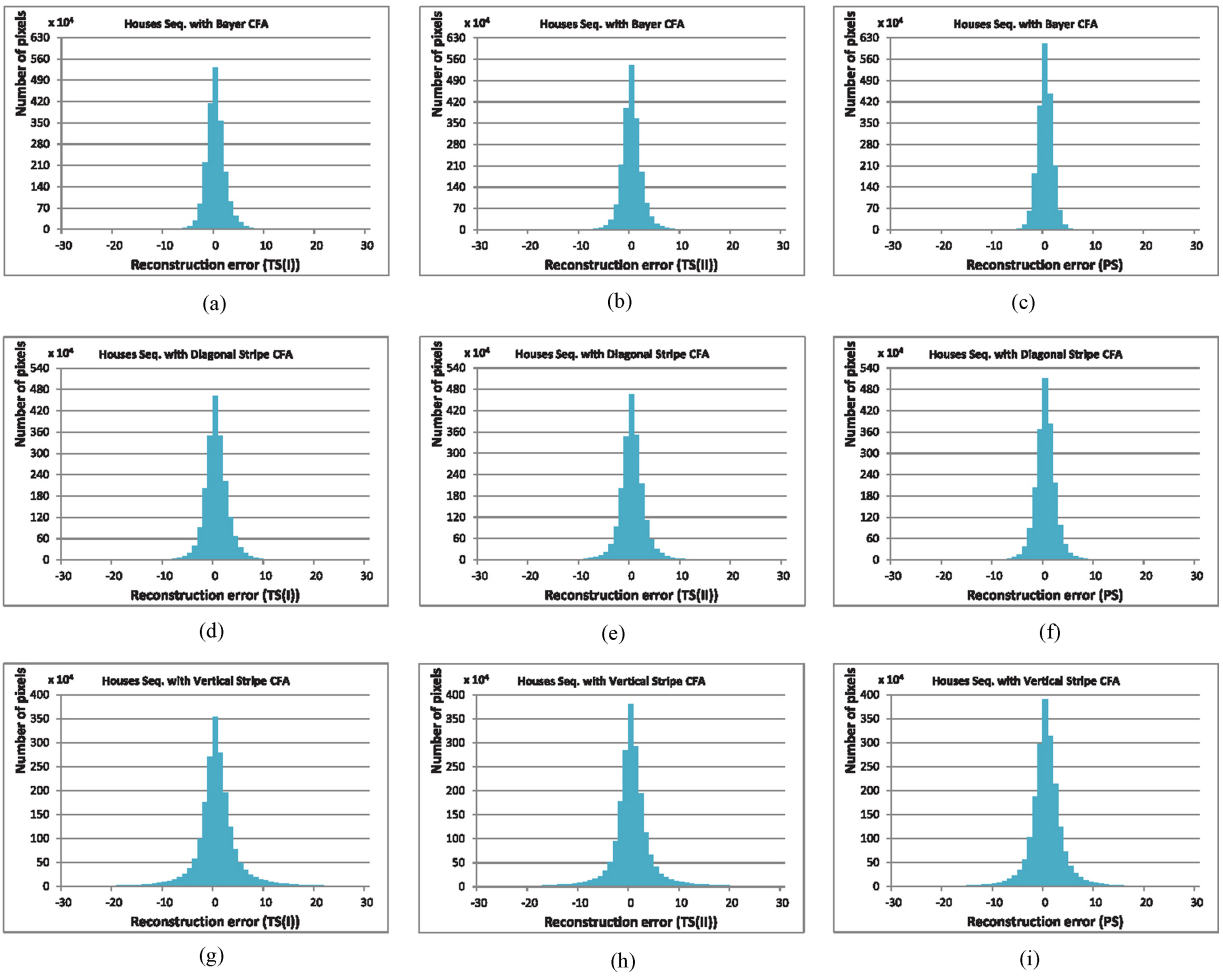

Fig. 17. Reconstruction error histograms for the *Houses* sequence. (a) TS(I) for the Bayer CFA structure. (b) TS(II) for the Bayer CFA structure. (c) PS for the Bayer CFA structure. (d) TS(I) for the diagonal stripe CFA structure. (e) TS(II) for the diagonal stripe CFA structure. (f) PS for the diagonal stripe CFA structure. (g) TS(I) for the vertical stripe CFA structure. (h) TS(II) for the vertical stripe CFA structure. (i) PS for the vertical stripe CFA structure.

Lukac and Plataniotis' universal demosaicing scheme (LD) and the proposed universal demosaicing scheme (PD), respectively. Three RD curves in each red and blue group represent the traditional subsampling strategy with format 4:2:0(I) [TS(I)], the traditional subsampling strategy with format 4:2:0(II) [TS(II)], and the proposed universal subsampling strategy (PS), respectively. It is clear that for different values of bitrate, integration of the proposed universal demosaicing scheme and chroma subsampling strategy always delivers better video sequence quality in terms of PSNR. For the case of using the same subsampling scheme, the proposed universal demosaicing strategy always gives higher PSNR. As for the case of using the same demosaicing strategy, the proposed universal subsampling scheme always gives higher PSNR.

Furthermore, Figs. 10–16 also demonstrate the effect of the proposed universal demosaicing scheme and chroma subsampling strategy on the quality of the reconstructed mosaic video sequences when classifying the CFA structures into three categories. For the first category including the Bayer CFA, Lukac and Plataniotis CFA, Yamanaka CFA, and modified Bayer CFA, the demosaicing scheme plays a more significant role than the chroma subsampling strategy for the cases of low bitrate, whereas, for the cases of high bitrate, the chroma subsampling strategy has more significant effect than the demosaicing scheme. For the second category including the diagonal stripe CFA and HVS-based CFA, the demosaicing scheme plays a more significant role than the chroma subsampling strategy. For the last category of the vertical stripe CFA, the chroma subsampling strategy plays a more significant role than the demosaicing scheme. In summary, the demosaicing scheme and the chroma subsampling strategy have different significance for different CFA structures and the integration of the proposed universal demosaicing scheme and subsampling strategy always yields the best quality of the reconstructed video sequence.

Based on the RD curves shown in Figs. 10–16, the related gain, measured by Bjøntegaard delta PSNR (BD-PSNR) and Bjøntegaard delta bitrate (BD-BR) [2], [33], of the proposed universal chroma subsampling strategy over the two traditional subsampling strategies is calculated and tabulated in Table III. As suggested by Video Coding Experts Group [35], BD-PSNR measures the average gain in PSNR under similar values of bitrate, whereas BD-BR measures the average gain in bitrate under similar values of PSNR. In Table III, the positive values of BD-PSNR and BD-BR, respectively, indicate that the proposed universal chroma subsampling strategy delivers

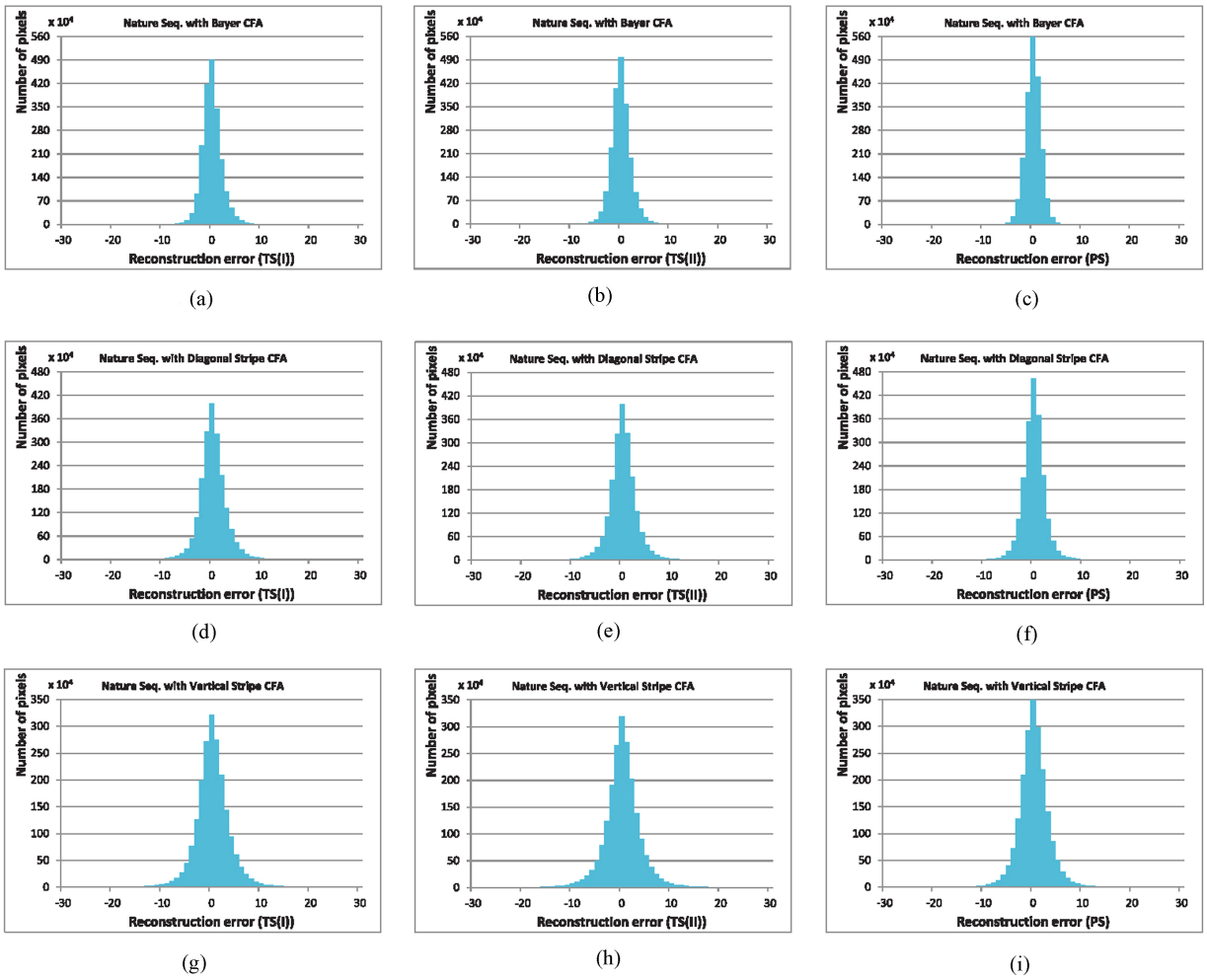

Fig. 18. Reconstruction error histograms for the *Nature* sequence. (a) TS(I) for the Bayer CFA structure. (b) TS(II) for the Bayer CFA structure. (c) PS for the Bayer CFA structure. (d) TS(I) for the diagonal stripe CFA structure. (e) TS(II) for the diagonal stripe CFA structure. (f) PS for the diagonal stripe CFA structure. (g) TS(I) for the vertical stripe CFA structure. (h) TS(II) for the vertical stripe CFA structure. (i) PS for the vertical stripe CFA structure.

higher PSNR and lower bitrate than the compared strategy. Thus, it is clear that under the same demosaicing strategy, the proposed universal subsampling scheme always yields higher PSNR and lower bitrate, especially in the low QP situation.

For comparison at the pixel level, we constructed the histograms of the reconstruction errors based on the *House* and *Nature* video sequences. For simplicity, one CFA structure from each of the three categories mentioned above was used to evaluate the reconstruction errors. Specifically, to demonstrate the effectiveness of the proposed subsampling strategy, Figs. 17 and 18 show the histograms of the reconstruction errors corresponding to the proposed universal demosaicing scheme integrated with three chroma subsampling strategies when stetting QP to be 12 (although it is applicable to different QPs). It is observed that the proposed chroma subsampling strategy always generates sharper Laplacian distributions of the reconstruction errors, implying that the proposed universal chroma subsampling strategy delivered better quality of the reconstructed video sequences.

In addition to the objective metrics, the subjective visual evaluation was used to demonstrate the effectiveness of the proposed universal chroma subsampling on the detailed texture regions. Mosaic image frames taken from the *Houses* video sequence were used for evaluation. Chroma subsampling often generates sampling distortion on texture regions in the reconstructed mosaic image frames and results in the degradation in the visual perception. To show the sampling distortion on texture regions more clearly, the color value of each pixel is represented by its corresponding gray-level value. Fig. 19(a)–(d) shows, in the gray-level value, the magnified subimages of the original mosaic image frame and the corresponding reconstructed mosaic subimages generated by two traditional subsampling strategies and the proposed universal chroma subsampling strategy, respectively. It is clear that the proposed universal chroma subsampling strategy yields less sampling distortion when compared with the two traditional subsampling strategies, especially in the texture regions circled by the red lines, leading to better visual effect.

C. Computational Time of Each Step in the Proposed Compression Method

To demonstrate the feasibility of the proposed method, the computational time of the proposed compression method, including the demosaicing step, the subsampling step, and the H.264 encoding step, should be addressed. Since the computational time of the H.264 encoding step usually de-

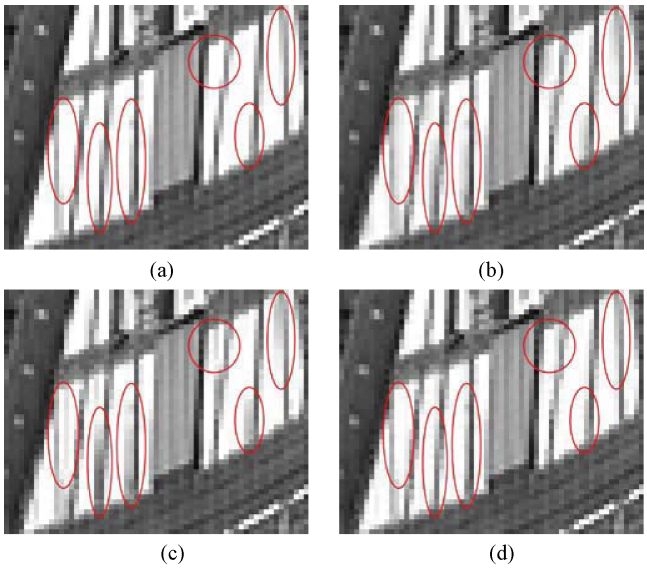

Fig. 19. Based on *Houses* video sequence with vertical stripe CFA structure. (a) Magnified subimages of the original mosaic image frame. Corresponding reconstructed mosaic subimages generated by (b) TS(I), (c) TS(II), and (d) PS.

TABLE IV
AVERAGE COMPUTATIONAL TIME (S) OF EACH STEP FOR PROCESSING AN IMAGE FRAME OF THE SIX TEST SEQUENCES WITH DIFFERENT CFA STRUCTURES

	Step			
	Demosaicing	Subsampling	H.264 Encoding	
CFA Structure			QP=8	QP=32
Bayer	0.2162	0.0182	3.8058	3.2800
Lukac and Plataniotis	0.2468	0.0182	3.9542	3.4282
Yamanaka	0.2629	0.0182	3.9447	3.4051
Diagonal stripe	0.1928	0.0182	3.7832	3.4924
Vertical stripe	0.1895	0.0171	3.8824	3.7248
Modified Bayer	0.1814	0.0170	3.9973	3.4933
HVS based	0.2328	0.0176	4.1785	3.5683
Average	0.2175	0.0178	3.9351	3.4846

creases progressively with the increase in the values of QP, we specifically consider the computational time for the cases of QP = 8 and QP = 32. Table IV gives the average computational time of each step for processing an image frame of the sequences with different CFA structures. It is obvious that the average computational time required for compressing an image frame is less than 4.5 s, indicating that the proposed compression method is effective. Furthermore, the computational time corresponding to the demosaicing and subsampling steps are much shorter than that of the H.264 encoding step, implying that the proposed universal demosaicing scheme and subsampling strategy are feasible.

VI. CONCLUSION

We proposed a universal chroma subsampling strategy for compressing mosaic video sequences with arbitrary RGB CFAs. We first developed a modified demosaicing scheme, which specifically recovered the G component in the color difference domain for recovering the missing color components to obtain the demosaiced video sequence with better quality. Based on the transform between the RGB and YUV color spaces, the proposed universal strategy properly sample, by considering the significance of the U and V components for reconstructing R and B pixels, the U and V chroma components, leading to better quality of the reconstructed mosaic video sequences. To the best of our knowledge, this is the first universal compression method designed specifically for mosaic video sequences with arbitrary RGB-CFAs. The experimental results on the mosaic video sequences with common types of the RGB-CFAs demonstrated that the proposed universal chroma subsampling strategy delivered better quality of the reconstructed mosaic video sequences when compared with the conventional strategy of H.264/AVC. Moreover, integrating the proposed universal demosaicing scheme and chroma subsampling strategy can deliver better video sequence quality. Although the proposed method performs well in most types of the RGB-CFAs, for video sequences with the vertical stripe CFA, the proposed method still cannot avoid the color artifacts in the regions with vertical texture due to the limitations on the mosaic structure. Furthermore, since the proposed method is designed for the RGB-CFAs, it is interesting to extend the results of this paper to deal with the non-RGB CFAs [17].

REFERENCES

[1] B. E. Bayer, "Color imaging array," U.S. Patent 3 971 065, 1976.
[2] G Bjøntegaard, "Calculation of average PSNR differences between RD curves," document VCEG Contribut. VCEG-M33, Austin, TX, 2001.
[3] E. Bodenstorfer, J. Fürtler, J. Brodersen, K. J. Mayer, C. Eckel, K. Gravogel, and H. Nachtnebel, "High speed line-scan camera with digital time delay integration," in *Proc. Electron. Imag. Conf. Real Time Imag.*, vol. 6496. 2007, pp. 1–10.
[4] H. Chen, M. Sun, and E. Steinbach, "Compression of Bayer-pattern video sequences using adjusted chroma subsampling," *IEEE Trans. Circuits Syst. Video Technol.*, vol. 19, no. 12, pp. 1891–1896, Dec. 2009.
[5] K. H. Chung and Y. H. Chan, "Color demosaicking using variance of color differences," *IEEE Trans. Image Process.*, vol. 15, no. 10, pp. 2944–2955, Oct. 2006.
[6] K. L. Chung, W. J. Yang, W. M. Yan, and C. C. Wang, "Demosaicing of color filter array captured images using gradient edge detection masks and adaptive heterogeneity-projection," *IEEE Trans. Image Process.*, vol. 17, no. 12, pp. 2356–2367, Dec. 2008.
[7] K. L. Chung, W. J. Yang, P. Y. Chen, W. M. Yan, and C. S. Fuh, "New joint demosaicing and zooming algorithm for color filter array," *IEEE Trans. Consumer Electron.*, vol. 55, no. 3, pp. 1477–1486, Mar. 2009.
[8] K. L. Chung, W. J. Yang, W. M. Yan, and C. S. Fuh, "New joint demosaicing and arbitrary-ratio resizing algorithm for color filter array using DCT approach," *IEEE Trans. Consumer Electron.*, vol. 56, no. 2, pp. 783–791, Feb. 2010.
[9] K. L. Chung, W. J. Yang, J. H. Yu, W. M. Yan, and C. S. Fuh, "Novel quality-effective zooming algorithm for color filter array," *J. Electron. Imag.*, vol. 19, no. 1, p. 013005, 2010.
[10] K. L. Chung, W. J. Yang, C. H. Chen, H. Y. M. Liao, and S. M. Zeng, "Efficient chroma subsampling strategy for compressing DTDI mosaic video sequences in H.264/AVC," *J. Electron. Imag.*, vol. 20, no. 2, p. 023011, 2011.
[11] C. Doutre and P. Nasiopoulos, "An efficient compression scheme for colour filter array video sequences," in *Proc. IEEE 8th Workshop Multimedia Signal Process.*, Oct. 2006, pp. 166–169.
[12] C. Doutre, P. Nasiopoulos, and K. N. Plataniotis, "H.264-based compression of Bayer pattern video sequences," *IEEE Trans. Circuits Syst. Video Technol.*, vol. 18, no. 6, pp. 725–734, Jun. 2008.
[13] C. Doutre and P. Nasiopoulos, "Modified H.264 Intra prediction for compression of video and images captured with a color filter array," in *Proc. IEEE ICIP*, Nov. 2009, pp. 3401–3404.
[14] *Draft ITU-T Recommendation and Final Draft International Standard of Joint Video Specification*, document ITU-T Rec. H.264/ISO/IEC 14 496-10 AVC, Joint Video Team of ISO/IEC and ITU-T, 2003.

[15] F. Gastaldi, C. C. Koh, M. Carli, A. Neri, and S. K. Mitra, "Compression of videos captured via bayer patterned color filter arrays," in *Proc. 13th Eur. Signal Process. Conf.*, 2005, pp. 983–992.
[16] B. Gunturk, Y. Altunbasak, and R. Mersereau, "Color plane interpolation using alternating projections," *IEEE Trans. Image Process.*, vol. 11, no. 9, pp. 997–1013, Sep. 2002.
[17] K. Hirakawa and P. J. Wolfe, "Spatio-spectral color filter array design for optimal image recovery," *IEEE Trans. Image Process.*, vol. 17, no. 10, pp. 1876–1890, Oct. 2008.
[18] R. W. G. Hunt, *Measuring Colour*, 2nd ed. Chichester, U.K.: Ellis Horwood, 1995.
[19] *Generic Coding of Moving Pictures and Associated Audio (MPEG-2)*, document ISO/IEC 13818, 1995.
[20] K. Jack, *Video Demystified: A Handbook for the Digital Engineer*, 5th ed. Eagle Rock, VA: LLH Technology Publishing, 2005.
[21] J. S. J. Li and S. Randhawa, "Color filter array demosaicking using high-order interpolation techniques with a weighted median filter for sharp color edge preservation," *IEEE Trans. Image Process.*, vol. 18, no. 9, pp. 1946–1957, Sep. 2009.
[22] W. Lu and Y. P. Tang, "Color filter array demosaicking: New method and performance measures," *IEEE Trans. Image Process.*, vol. 12, no. 10, pp. 1194–1210, Oct. 2003.
[23] R. Lukac, K. Martin, and K. N. Plataniotis, "Digital camera zooming based on unified CFA image processing steps," *IEEE Trans. Consumer Electron.*, vol. 50, no. 1, pp. 15–24, Jan. 2004.
[24] R. Lukac and K. N. Plataniotis, "Normalized color-ratio modeling for CFA interpolation," *IEEE Trans. Consumer Electron.*, vol. 50, no. 2, pp. 737–745, Feb. 2004.
[25] R. Lukac and K. N. Plataniotis, "Color filter arrays: Design and performance analysis," *IEEE Trans. Consumer Electron*, vol. 51, no. 4, pp. 1260–1267, Apr. 2005.
[26] R. Lukac and K. N. Plataniotis, "Universal demosaicking for imaging pipelines with an RGB color filter array," *Patt. Recognit.*, vol. 38, no. 11, pp. 2208–2212, 2005.
[27] R. Lukac and K. N. Plataniotis, "Data-adaptive filters for demosaicking: A framework," *IEEE Trans. Consumer Electron.*, vol. 51, no. 2, pp. 560–570, Feb. 2005.
[28] R. Lukac and K. N. Plataniotis, "Fast video demosaicking solution for mobile phone imaging applications," *IEEE Trans. Consumer Electron.*, vol. 51, no. 2, pp. 675–681, Feb. 2005.
[29] R. Lukac, K. N. Plataniotis, D. Hatzinakos, and M. Aleksic, "A new CFA interpolation framework," *Signal Process.*, vol. 86, no. 7, pp. 1559–1579, Jul. 2006.
[30] R. Lukac, *Single-Sensor Imaging: Methods and Applications for Digital Cameras*. Boca Raton, FL: CRC Press/Taylor & Francis, 2008.
[31] D. Menon and G. Calvagno, "Regularization approaches to demosaicking," *IEEE Trans. Image Process.*, vol. 18, no. 10, pp. 2209–2220, Oct. 2009.
[32] M. Parmar and S. J. Reeves, "A perceptually based design methodology for color filter arrays," in *Proc. IEEE ASSP*, vol. 3. May 2004, pp. 473–476.
[33] S. Pateux and J. Jung, "An excel add-in for computing Bjøntegaard metric and its evolution," document VCEG-AE07, VCEG, Marrakech, Morocco, 2007.
[34] S. C. Pei and I. K. Tam, "Effective color interpolation in CCD color filter arrays using signal correlation," *IEEE Trans. Circuits Syst. Video Technol.*, vol. 13, no. 6, pp. 503–513, Jun. 2003.
[35] T. K. Tan, G. Sullivan, and T. Wedi, "Recommended simulation conditions for coding efficiency experiments," document VCEG contribution VCEG-AA10, Nice, France, 2005.
[36] S. Yamanaka, "Solid state camera," U.S. Patent 4 054 906, 1977.
[37] W. J. Yang, K. L. Chung, and H. Y. M. Liao, "Quality-efficient demosaicing for digital time delay and integration images using edge-sensing scheme in color difference domain," *J. Vis. Commun. Image Representat.*, vol. 23, no. 5, pp. 729–741, May 2012.
[38] W. J. Yang, K. L. Chung, and H. Y. M. Liao, "Efficient reversible data hiding for color filter array images," *Inform. Sci.*, vol. 190, pp. 208–226, May 2012.
[39] W. J. Yang, K. L. Chung, W. N. Yang, and L. C. Lin. *The Experimental Results of Universal Chroma Subsampling Strategy for Compressing Mosaic Video Sequences With Arbitrary RGB Color Filter Arrays in H.264/AVC* [Online]. Available: http://140.118.175.164/WJYang/paper/RGBCFA Compression
[40] Fraunhofer Heinrich Hertz Institute. *H.264/AVC Reference Software* [Online]. Available: http://iphome.hhi.de/suehring/tml/download/old_jm

Wei-Jen Yang received the B.S. degree in computer science and information engineering from the National Taiwan University of Science and Technology, Taipei, Taiwan, in 2004, and the Ph.D. degree in computer science and information engineering from National Taiwan University, Taipei, in 2009.

He is currently a Post-Doctoral Researcher with the Department of Computer Science and Information Engineering, National Taiwan University of Science and Technology. His current research interests include color image processing, digital camera image processing, data hiding, image or video compression, computer vision, pattern recognition, and algorithms.

Dr. Yang was a recipient of the Best Paper Award from the Society of Computer Vision, Graphics, and Image Processing, Taiwan, in 2007, and the Ph.D. Dissertation Award from the Institute of Information and Computing Machinery, Taiwan, in 2010.

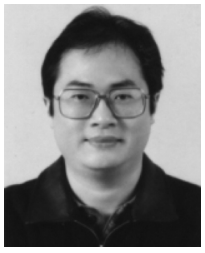

Kuo-Liang Chung (M'91–SM'01) received the B.S., M.S., and Ph.D. degrees from National Taiwan University, Taipei, Taiwan, in 1982, 1984, and 1990, respectively.

He is currently a Professor with the Department of Computer Science and Information Engineering, National Taiwan University of Science and Technology (NTUST), Taipei, Taiwan, where he's been since 1995. After two years of obligatory military service from 1984 to 1986, he was a Research Assistant with the Institute of Information Science at Academia Sinica, Taiwan, from 1986 to 1987. He was a Visiting Scholar with the University of Washington, Seattle, in 1999. From 2003 to 2006, he was the Chair of the Department of Computer Science and Information Engineering, NTUST. Since 2009, he has been a University Chair Professor with NTUST. His current research interests include image or video compression, image or video processing, pattern recognition, 3-D video processing, and shape analysis in computer vision.

Dr. Chung was a recipient of the Distinguished Research Award from the National Science Council of Taiwan in 2004, the Best Paper Award from the Image Processing and Pattern Recognition Society of Taiwan in 2007, and the Distinguished Teaching Award of NTUST in 2009. He was a Managing Editor of the *Journal of Chinese Institute of Engineers* from January 1996 to December 1998. In August 2000, he was the Program Co-Chair of the Conference on Computer Vision, Graphics, and Image Processing, Taiwan. He is currently an Associate Editor of the *Journal of Visual Communication and Image Representation*. He is a fellow of the Institute of Engineering and Technology.

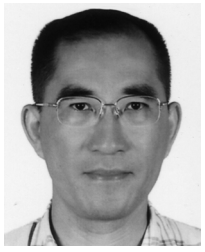

Wei-Ning Yang received the Ph.D. degree in industrial and systems engineering from Ohio State University, Columbus.

He is currently an Associate Professor with the Department of Information Management, National Taiwan University of Science and Technology, Taipei, Taiwan. His current research interests include statistical analysis, stochastic simulation, and image processing.

Le-Chung Lin received the B.S. and M.S. degrees in computer science and information engineering from the National Taiwan University of Science and Technology, Taipei, in 2010 and 2012, respectively.

His current research interests include image or video compression, image or video processing, pattern recognition, and 3-D video processing.

Mr. Lin is an Honorary Member of the Phi Tau Phi Scholastic Honor Society, Taiwan.